Robust Manipulation of Magnetism in Dilute Magnetic Semiconductor (Ga,Mn)As by Organic Molecules

Xiaolei Wang, Hailong Wang, Dong Pan, Timothy Keiper, Lixia Li, Xuezhe Yu, Jun Lu, Eric Lochner, Stephan von Molnár, Peng Xiong, and Jianhua Zhao**

A distinguishing characteristic of a semiconductor is the great tunability of its physical properties via variation of its carrier density by a variety of electrical, chemical, and optical means. In a magnetic semiconductor, the magnetic properties of the material may be controlled in a similar fashion, suggesting that ferromagnetism could be manipulated by nonmagnetic means. In the case of III–V dilute magnetic semiconductors (DMSs), the holes from Mn doping are known to mediate the ferromagnetic interaction among the Mn ions.[1–3] Through modulation of the hole density, electrostatic gating or photoillumination has been shown to significantly alter the magnetic properties of (III, Mn)V films.[4–6]

Hybrid structures of functional molecules and solid-state materials have attracted extensive interest in the development of surface nanoscience and molecular electronics/spintronics. The formation and patterning of self-assembled monolayers (SAMs) of organic molecules on metal, semiconductor, and oxide surfaces[7–9] have been demonstrated via a variety of techniques. Molecular spintronics, the study of electronic spin transport through molecular media and barriers as well as molecule/solid-state interfaces,[10,11] has seen significant progress, as exemplified by the realization of organic spin-valves[12] and magnetic tunnel junctions,[13,14] spin filtering through chiral molecules,[15] and molecular spin memory devices.[16,17] The ferromagnetic–organic interface, as an essential component of molecular spintronic devices, has been the focus of many recent studies[18,19] due to the prospects of producing novel electrical and magnetic functionalities. So far, studies of molecular modification of magnetism have mostly focused on metals where the effects are limited to the surface because of the large carrier densities and short screening lengths:[17,20] Both theoretical calculations[19,21] and experiments[15,16,19] have revealed possible presence of large spin polarization and spin-filtering effect at the interface of nonmagnetic organic molecules and ferromagnetic metals. Such hybrid structures may also induce interfacial magnetization in the organic molecules[17] and modify the surface magnetic anisotropy of the ferromagnetic metals.[20] Even more intriguing, there have been a series of reports of induced magnetic moments, even ferromagnetism, on the surfaces of nonmagnetic metals through decoration of organic SAMs,[15,22] although a recent spin-polarized tunneling experiment has failed to find measureable spin polarization at a thiol–Au interface.[23]

In principle, DMSs are ideal candidates for significant molecular modification of magnetism due to their lower carrier densities and critical role of carrier-mediated ferromagnetism;[1–3] it is expected that the effect will not only be more pronounced but also extend over much larger depth because of the significantly longer screening length in semiconductors. So far, modification of magnetic properties in (III, Mn)V films has been primarily through electrostatic[4–6] and ferroelectric[24] field-effect gating or photoillumination[25] through modulation of the hole density. An obvious choice for such studies is (Ga,Mn)As, which is the most thoroughly investigated DMS material. There have been surprisingly few experimental efforts in using organic molecules to manipulate the magnetic properties of DMSs. A primary reason behind the scarcity may be the difficulty of creating high-quality SAMs on III–V DMSs. One such work[26] demonstrated robust modification of ferromagnetism in a semiconducting ferromagnet by adsorption of monolayers of alkylphosphonic acids on a GaAs cap layer via a phosphonate group. However, the material is a heterogeneous ½ monolayer MnAs buried below 5 nm of GaAs and only suppression of ferromagnetism is shown. On the other hand, surface organic molecules are shown to be effective in tuning the critical temperatures of thin films of cuprate superconductors,[27] materials with similar carrier concentrations as DMSs.

In this work, a new method for effective manipulation of the ferromagnetism of (Ga,Mn)As is develped; a prototypical DMS: Organic molecules were deposited on the surface of (Ga,Mn)As films by either solution-based self-assembly or vacuum deposition, which led to large carrier density modulation, and significant changes in the Curie temperature (T_C) and saturation magnetization (M_s). Both electron acceptor and donor molecules were tested and found to, respectively, enhance or reduce T_C in (Ga,Mn)As films with largest modulation up to 36 K. Our experimental results can be described by a modification of the p-d Zener model.[3] Moreover, a surface preparation protocol enables direct writing of nanopatterns of organic molecule self-assembled monolayers on (Ga,Mn)As surface by dip-pen nanolithography (DPN). These results point to the possibility of controlled nanoscale manipulation of magnetism in DMSs

Dr. X. Wang, Dr. H. Wang, Dr. D. Pan, L. Li,
Dr. X. Yu, Dr. J. Lu, Prof. J. Zhao
State Key Laboratory of Superlattices
and Microstructures
Institute of Semiconductors
Chinese Academy of Sciences
P.O. Box 912, Beijing 100083, China
E-mail: jhzhao@red.semi.ac.cn

T. Keiper, Dr. E. Lochner, Prof. S. von Molnár, Prof. P. Xiong
Department of Physics
Florida State University
Tallahassee, FL 32306, USA
E-mail: xiong@physics.fsu.edu

DOI: 10.1002/adma.201503547

via surface molecular patterning, which can be directly imaged with a magnetic scanning probe.

The (Ga,Mn)As thin films with thicknesses from 5 to 10 nm and nominal 4 at% Mn were grown on semi-insulating GaAs (001) substrates by low-temperature molecular-beam epitaxy (LT-MBE). A thiol molecule, 16-mercaptohexadecanoic acid (MHA), was used as the electron-donating species. Monolayer self-assembly of MHA on GaAs and (Ga,Mn)As is made possible with a solution treatment for oxide removal and surface passivation: The GaAs wafers or (Ga,Mn)As films were immersed in an ammonium sulfide solution for several minutes which not only etches away the native oxide but also leaves behind a sulfur passivation layer that greatly slows reoxidation of the film surface.[28,29] For p-type doping, we utilized 2,3,5,6-tetrafluoro-7,7,8,8-tetracyanoquinodimethane (F4-TCNQ), which has a strong electron affinity,[30] as a strong electron acceptor to increase the hole density in the (Ga,Mn)As. F4-TCNQ was thermally evaporated onto the (Ga,Mn)As films. It has been shown in a variety of n- or p-type materials[30–33] that the adsorption of F4-TCNQ leads to strong compensation of electron carriers, and in some cases the Fermi level is driven from the conduction band into the band gap. So for the p-type (Ga,Mn)As films, it is expected that F4-TCNQ will inject more holes into the material when adsorbed on the film surface.

Figure 1a shows a schematic representation of the passivation and MHA assembly process on (Ga,Mn)As: removing the native oxide layer by ammonium sulfide solution, formation of a sulfur passivation layer, and MHA SAM assembly. We have observed no differences on the assembly on GaAs and (Ga,Mn)As. A key step to the realization of high-quality MHA SAM on GaAs and (Ga,Mn)As is the preparation of a properly passivated oxide-free surface, for which we employed treatment by an ammonium polysulfide ($(NH_4)_2S_x$) solution. The effects of the sulfur-passivation and formation of MHA SAM on the treated surface were confirmed by X-ray photoelectron spectroscopy (XPS), high-resolution transmission electron microscopy (HRTEM) (see the Supporting Information), and DPN.

Previous studies[28,29] have shown that such a treatment by a diluted $(NH_4)_2S$ solution combined with additional elemental sulfur effectively removes native oxides from III–V semiconductor surfaces, and creates an atomic layer of sulfur covalently bonded to the fresh surface. The process results in much improved surface stability in air and prevents reoxidation for considerable time, sufficient for further processing. We observed that the sulfur-passivated surface serves as an excellent platform for the formation of high-quality SAMs of thiol molecules on GaAs and (Ga,Mn)As through exchange of the sulfur and the thiol terminal of the molecules.

Figure 1b shows the survey XPS scans of three GaAs samples cleaved from a semi-insulating GaAs wafer which had been stored in air for months. The first sample (green) was measured as-cut, the second sample (red) was immersed in a diluted 1% $(NH_4)_2S$ solution saturated with additional elemental sulfur at pH = 8.6 for 3 min, and the third sample (blue) was further immersed in a 1×10^{-3} M MHA ethanol solution for 1 min. Both the second and the third samples were exposed to ambient air for days between the final processing steps and the XPS measurement. From the survey spectra, the O 1s core level peak in the unpassivated (as-cut) sample reveals clear signatures of surface oxidation on the native surface, while those from the S-passivated and MHA-functionalized samples show diminished intensities. The Ga 3d and As 3d peaks (Figure 1c,d, respectively) exhibit doublet features due to oxide species on the unpassivated sample. In contrast, after S-passivation, the doublet features disappear and a single peak emerges with chemical shift to higher energies, which are considered spectroscopic signatures for the replacement of native oxide Ga and As species by specific Ga–S and As–S bonding components.[34] In Figure 1e,f, both the S 2s and 2p peaks show two sulfur species corresponding to Ga–S and As–S bonding present at the surface. The absence of spectral features at binding energy (BE) ≥ 163.5 eV in the S 2p region indicates that there are no free thiol groups in these films, which is consistent with the S-passivation and thiol binding, respectively. Between the S-passivated and MHA-functionalized samples, both the S 2s and S 2p peaks shift to lower energies, which is consistent with the shift in As 2p in Figure 1g, and indicates the thiolate effect and replacement of the S by the thiol in MHA. The As^{3+} and As^{5+} oxide peaks at BE of 1321.6 and 1324.8 eV, respectively, are observed in the unpassivated sample, but are absent in the S-passivated and MHA-functionalized samples, as shown in Figure 1g. After S-passivation, a distinct As–S component appears at BE of 1322.7 eV, which indicates the formation of As–S bond on GaAs;[35] with MHA functionalization, the As–S peak moves to BE of 1321.7 eV. A similar result was obtained for As 3d, with a second peak around 43–44 eV from As^{3+} in As_2O_3 and a sharper peak just above 40 eV from GaAs. A possible explanation for the difference between the S-passivated sample and the MHA-functionalized sample is the monovalent chemisorption of thiolated sulfur in the MHA sample. Additional evidence for the formation of MHA SAM is shown in Figure 1h: The C 1s spectrum shows double peaks at BE of 284.0 and 284.5 eV in the MHA-functionalized sample, which originates from the carbon chain in MHA for C–C/C–H bonds and a small peak around 286.0 eV for C-oxide peak. In contrast, the unpassivated and S-passivated samples show single peaks around 285.0 eV, which is characteristic of spurious carbon contaminations.[34]

Table 1 summarizes the surface atomic percent profiles calculated from the XPS spectra for the three samples. With 3 min of the ammonia sulfide treatment, the fraction of the O component decreases while S component increases steeply, indicating that S has replaced O on the surface which changes from As–O/Ga–O to As–S/Ga–S. It is evident that this solution treatment results in a much less oxidized surface. The small amount of O (≈8%) on the S-passivated sample may have come from reoxidation before the XPS measurement (days). Exchange of the S-passivation layer by an MHA SAM has no discernible effect on the surface composition, as expected from the chemical composition. However, MHA coverage immediately after S-passivation effectively minimizes the reoxidation as evidenced by the almost complete absence of O. We conclude that the XPS results provide strong evidence that the ammonia sulfide treatment prepared a clean, reactive S-passivated surface, which opened the way for exchange of S with the thiol termini and formation of high-quality MHA SAM.

The robustness of the process of MHA SAM assembly on the S-passivated GaAs and (Ga,Mn)As surfaces is further evidenced by successful DPN patterning. DPN,[36] a technique of direct

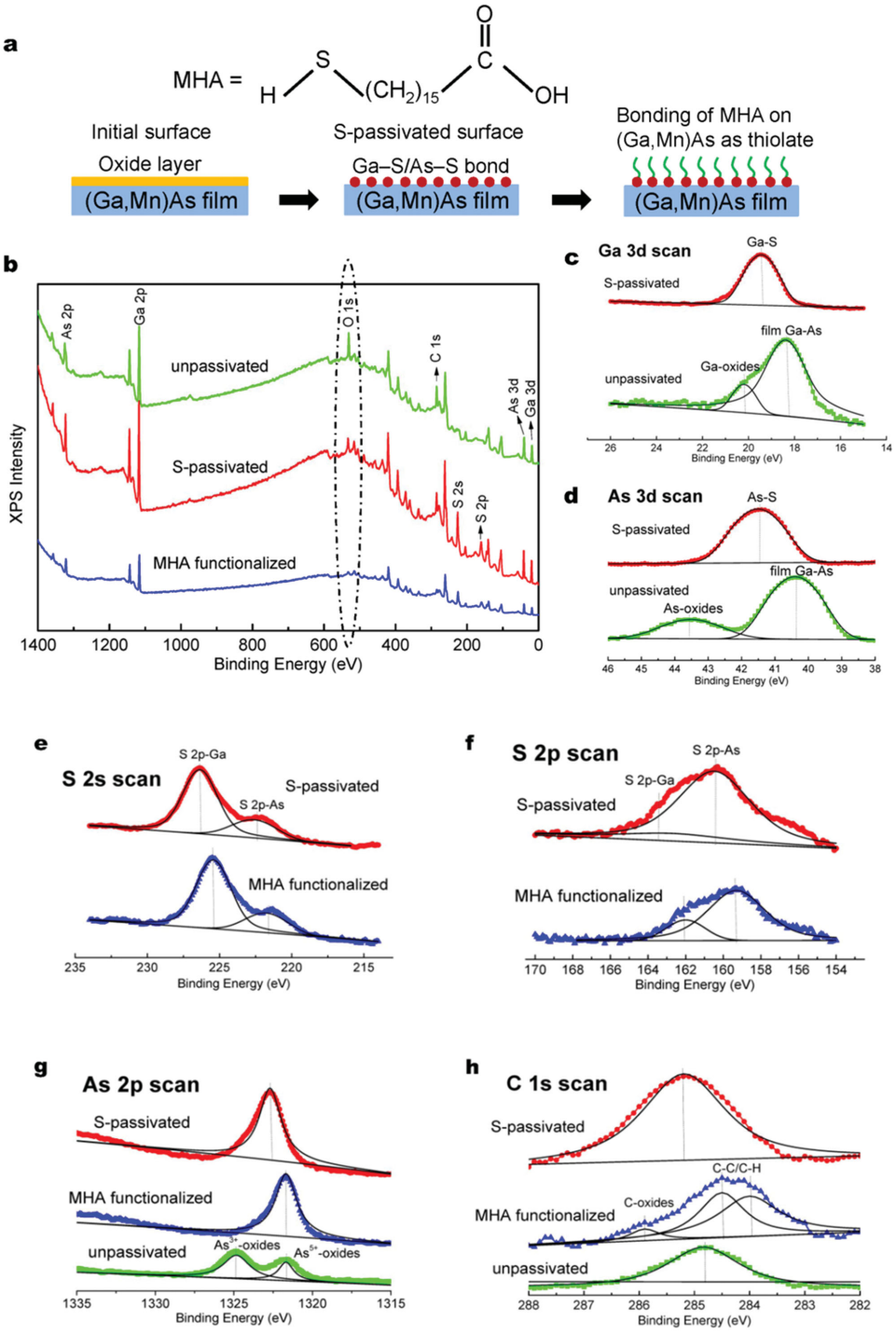

Figure 1. a) Schematic representation of the surface modification processes. b) Survey spectra of unpassivated, S-passivated, and MHA-functionalized GaAs samples. c) Close-ups of the Ga 3d core level spectra. d) Close-ups of the As 3d core level spectra. e) The S 2s spectra show two sulfur species (S 2s-Ga and S 2s-As). f) Peaks attributed to the S 2p core level, with the presence of specific S 2p-Ga and S 2p-As. g) The specific peaks of As 2p. h) The C 1s core level spectra. Component fits to the spectra are shown by black solid lines.

writing of nanoscale SAM patterns of organic molecules on a solid-state substrate by an atomic force microscope, requires close matching of the molecular "ink" and the surface of the solid-state "paper." The ability of the molecules to form an SAM on the substrate is a necessary but not sufficient condition for successful DPN. The transport and diffusion of the molecules are strongly dependent on the interaction between the molecular ink and substrate surface through the meniscus effect,[37] hence the combinations of organic molecules and solid-state substrates that yield successful DPN have been rather limited.

Table 1. Atomic percent profile of main elements on GaAs surface by XPS.

State of surface	Ga [%]	As [%]	S [%]	O [%]
Unpassivated	39.8	31.4	0	28.8
S-passivated	22.9	17.2	51.6	8.3
MHA functionalized	24.2	18.0	57.8	0

DPN has been realized most frequently by thiol molecules on noble metals (mostly Au),[36–38] and occasionally by silane molecules on oxidized semiconductor surfaces.[39–41] To the best of our knowledge, there has been no report of direct DPN of nanoscale organic SAM on a semiconductor free of surface oxide. Here, we show that the S-passivated surface enables direct writing of arbitrary SAM patterns of MHA on GaAs and (Ga,Mn)As. Shown in **Figure 2**b–d, are lateral force microscopy (LFM) images of MHA SAM patterns of a 3×3 μm^2 square, lines of different widths, and the chemical formula "GaMnAs," respectively. 3 min of treatment of the substrate by the sulfur-saturated ammonia sulfide solution was critical for DPN of MHA; DPN on substrates with no treatment or 1 min treatment produced no visible MHA patterns (see the Supporting Information). These results corroborate the conclusion drawn from the XPS study that the MHA SAM patterns materialize through exchange of the sulfur in As–S/Ga–S with the thiol in MHA. The MHA molecules are thus expected to act as electron donors, which should compensate the holes in the (Ga,Mn)As films.

Carrier modulation of opposite polarity was achieved by depositing the strong electron-acceptor molecule, F4-TCNQ, on the (Ga,Mn)As surface via high vacuum thermal evaporation. The hole injection into the (Ga,Mn)As films is attributed to the interfacial energy level alignment with the F4-TCNQ[7,31,33] and the resulting electron transfer from the (Ga,Mn)As film to F4-TCNQ. This is confirmed through extensive XPS measurements on (Ga,Mn)As films with 0, 1, and 3 monolayers of F4-TCNQ on the surface. The details are presented in the Supporting Information. A central observation was the appearance of the N^{-1} anion species with coverage of F4-TCNQ, which indicates that the electron transfer takes place through the C≡N groups of the molecules, and the dominant N^{-1} spectral feature comes from the Ga–N bonds at the interface.

After establishing the charge transfer between (Ga,Mn)As and the surface molecular layers (MHA and F4-TCNQ), we explored the modulation of ferromagnetism in the (Ga,Mn)As films by the organic molecules. Magnetic and magnetotransport measurements were performed in a commercial superconducting quantum interference device (SQUID) magnetometer and physical property measurement system (PPMS), respectively. The magnitude and polarity of the charge transfer across the interfaces of the MHA/(Ga,Mn)As and F4-TCNQ/(Ga,Mn)As were determined directly via Hall measurements. **Figure 3** shows a representative set of results exemplifying the effects of the molecular modifications on the magnetic and magnetotransport properties [$M(T)$, $M(H)$, $\rho_{xx}(T)$, and $\rho_{xy}(H)$] for a 9 nm thick (Ga,Mn)As film with 1 nm GaAs cap layer. The data are presented for the as-grown (black), F4-TCNQ deposited (red), and MHA-functionalized (blue) samples, each of 6×7 mm^2 rectangular geometry. In this work, GaAs cap layers up to 2 nm thick (e.g., 1 nm cap for the sample in Figure 3) were grown on some of the (Ga,Mn)As films in order to minimize potential spurious effects from unintended surface contamination/reaction. However, comparison of results with samples without a GaAs cap layer (e.g., samples shown in the Supporting Information) shows little difference. Also, there may be small defects in the organic layers, however, such defects should have minimal effect on the T_C modulation. This is supported by the observation that increasing the immersion time in the MHA solution beyond 1 min and depositing more than 1 nm of F4-TCNQ had no measurable effect on the T_C modulation.

The $M(T)$ data (Figure 3a) reveal clear changes of T_C resulting from the surface molecular coverages: the F4-TCNQ enhances T_C, while the MHA reduces T_C. Quantitatively, T_C was determined from the peak temperature of dM/dT, as shown in the inset. Interestingly, $M(H)$ measurements at low temperatures (Figure 3b) revealed a similar trend in the saturation magnetization (M_s), which is increased upon F4-TCNQ deposition and diminished with MHA assembly on the surface. In all cases, the diamagnetic contributions from the GaAs substrate and buffer layer are subtracted by using the high-field slopes. Similar manifestations for the surface molecule induced changes of the carrier concentration can be found in the longitudinal

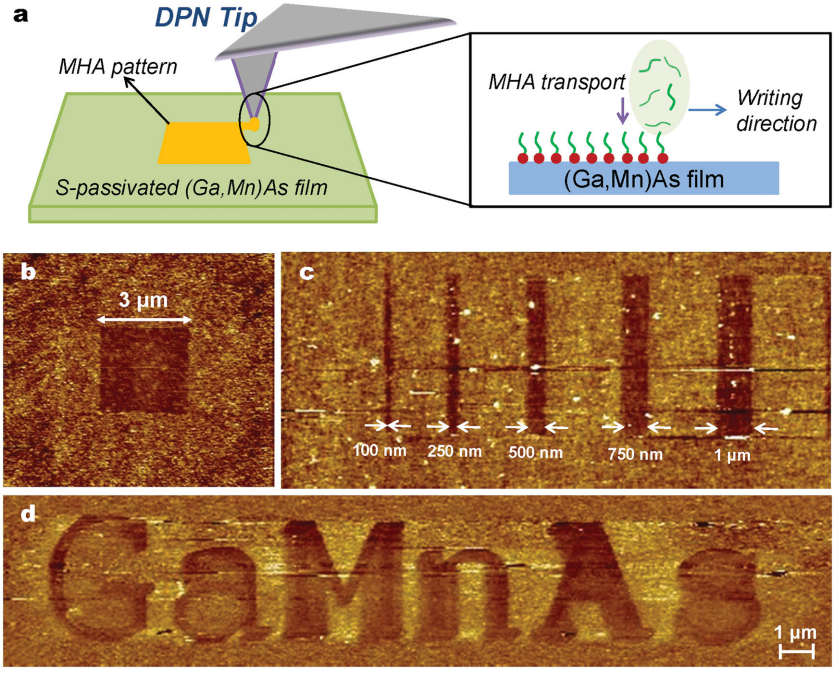

Figure 2. a) Schematics of the process of patterning MHA SAM on (Ga,Mn)As films by DPN. b) Lateral force microscopy (LFM) images of a 3×3 μm^2 square. c) Lines of widths 100 nm, 250 nm, 500 nm, 750 nm, and 1 μm. d) A pattern of the chemical formula "GaMnAs."

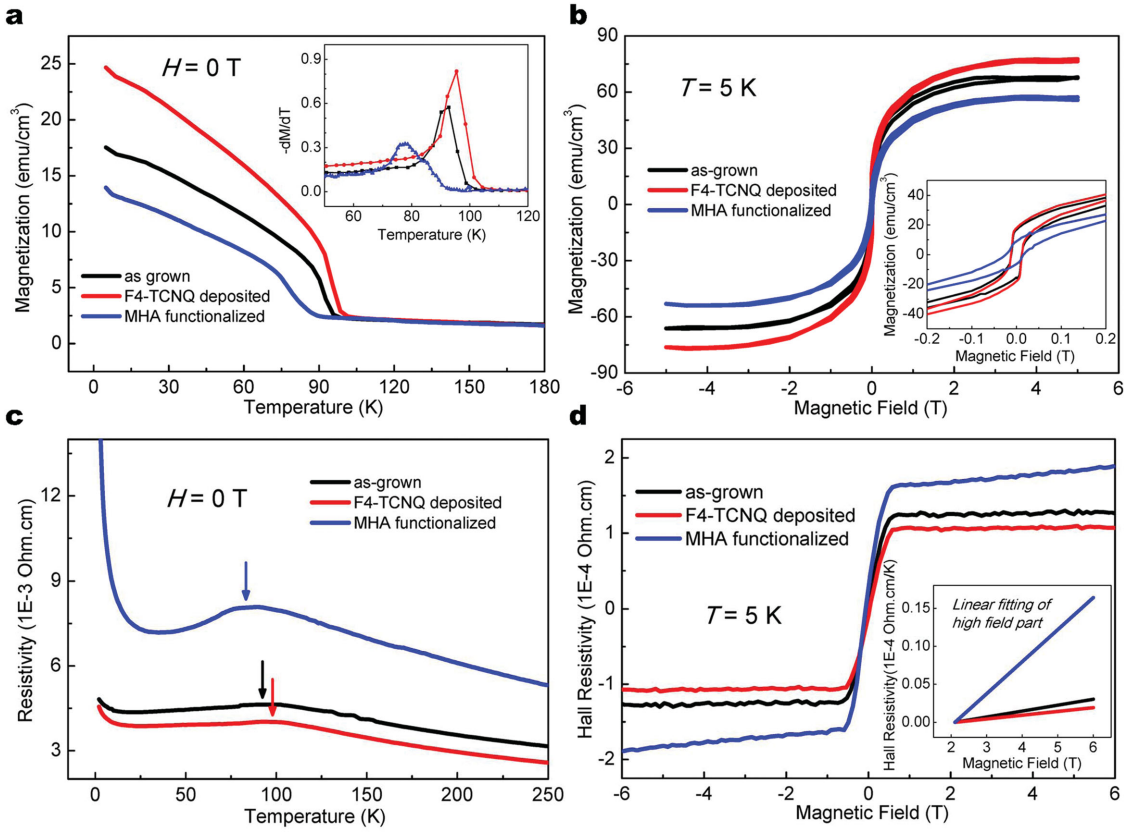

Figure 3. Molecular modifications on a 9 nm (Ga,Mn)As film with 1 nm GaAs cap layer indicated by a) temperature dependence of remnant magnetization, $M(T)$, taken at $H = 0$ T. Inset: dM/dT plots show more directly the variation of T_C of the three films. b) Magnetization hysteresis loops, $M(H)$, at 5 K, for the same three films. Inset: Close-up of the low field region. c) Temperature dependence of the longitudinal resistivity, $\rho_{xx}(T)$. d) Hall resistivity, $\rho_{xy}(H)$, taken at 5 K for the same three films. Inset: Linear fittings of the high field data which evidence the variation of the hole concentration resulting from surface molecules.

resistivity $\rho_{xx}(T)$ shown in Figure 3c. The Hall resistivity curves in Figure 3d show a pronounced anomalous Hall component at low fields. The high-field slopes are positive and yield a hole density of 8.9×10^{20} cm^{-3} for the as-grown sample, which decreases (increases) to 1.35×10^{20} cm^{-3} (1.45×10^{21} cm^{-3}) with the deposition of MHA (F4-TCNQ). The correlation between the hole concentration and resistivity is qualitatively in agreement with expectation and previous works.[42,43] Quantitatively, the changes in the resistivity are always smaller than what is expected from the carrier density variation, implying that there is a deterioration of the mobility upon adsorption of either type of molecules. This is probably due to the additional ionized impurity scattering introduced by the covalent bonding of the organic molecules to the (Ga,Mn)As. This may be additional evidence that the carrier density modulation in our systems originates from charge transfer due to the covalent bonding rather than from dipole electric field.[27] In addition, the T_C's inferred from $\rho_{xx}(T)$[44] (Figure 3c) show similar trends of variation with the molecular coverages as revealed by the magnetic measurements.

To gain a systematic and quantitative understanding of the degree of the molecular modulation of the ferromagnetism in the (Ga,Mn)As films, we studied a series of 4% Mn-doped (Ga,Mn)As films with different film and cap layer thicknesses. T_C and hole concentration were determined from dM/dT and Hall slopes, respectively, on the same films with and without molecular decorations. The results are plotted on log–log scales in **Figure 4**a with the error bars reflecting uncertainties in the Hall effect data. Theoretically, the p-d Zener model for ferromagnetism in DMSs predicts a power law scaling between T_C and hole concentration, with an exponent γ between 0.6 and 0.8 in the relevant range of hole densities.[3,45] However,[1,2] for thinner films (<5 nm) in the field-effect transistor structure, the exponents are found to be around 0.2, which is explained by considering the nonuniform distribution of the hole concentration along the out-of-plane (z) direction.[6] In our case, experimentally, the exponents were determined by examining the correlation of T_C with p for each sample upon molecular modifications (each color in Figure 4a); the number of data points for each sample is thus limited by the possible ways of molecular modification. The extracted exponents are plotted in the inset, and several features are worth noting in the data: For the thinnest (5 nm) sample with largest T_C modulation up to 36 K, $\gamma \approx 0.17$ was observed, which is close to the typical value obtained in the gating experiments.[6] γ decreases sharply with increasing thickness and is smaller than 0.12 for all 9 nm samples or thicker ones. Moreover, for the three 9 nm samples, γ is essentially the same despite the large differences in the starting

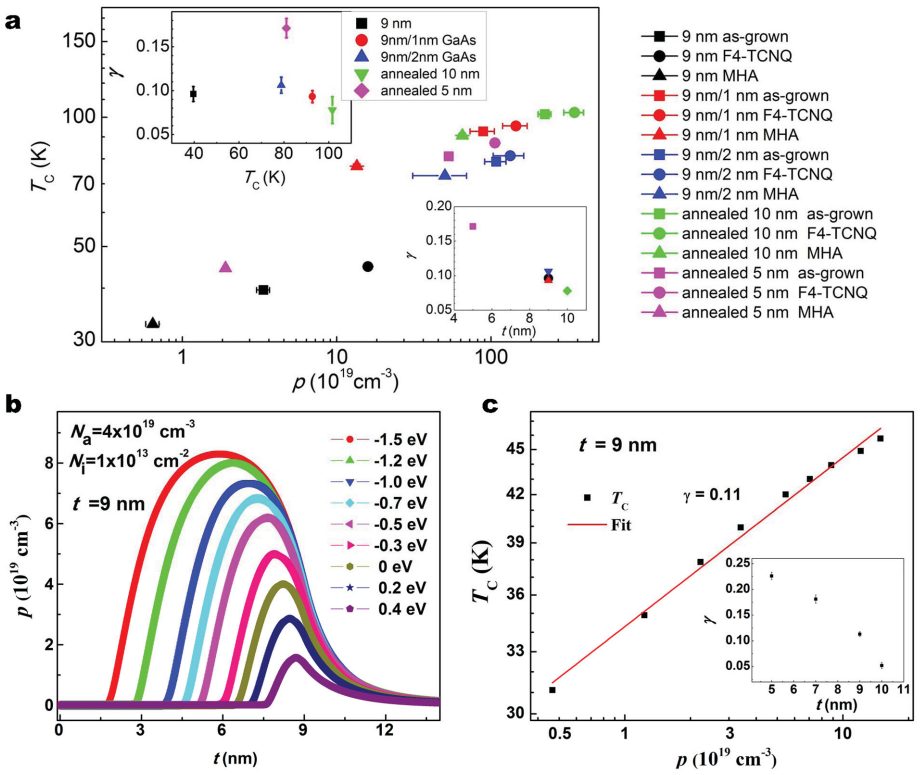

Figure 4. a) Log–log plot of T_C as a function of hole concentration p for five groups of (Ga,Mn)As films. The upper inset shows the power-law exponent γ determined from each group plotted against the T_C of the as-grown sample, while the lower inset indicates γ as a function of thickness t. b) Simulated variation of the hole density along z-direction, $p(z)$, for a 9 nm thick (Ga,Mn)As film with various ΔE, the energy difference between the Fermi energy of the (Ga,Mn)As and the HOMO of the molecules. c) Log–log plot of the calculated T_C versus average hole density from the simulations in (b). Inset: resulting critical exponent γ for four different film thicknesses.

T_C (39.6 K) and hole density (1.35×10^{19} cm^{-3}) for the as-grown samples. These observations strongly suggest that the film thickness is the primary factor determining the extent of the molecular modulation of the ferromagnetism in the (Ga,Mn)As, possibly due to the differing hole density gradients in films of different thicknesses from the charge transfer from the surface molecular layers.

To account for our experimental results, we invoke a mechanism similar to that for the field-effect transistor structure, in which the screening effect during the charge transfer process causes a nonuniform distribution of the hole concentration in the z-direction. Shown in Figure 4b,c are results of a numerical simulation based on the modified p-d Zener model, in which T_C is expressed as:[6]

$$T_C = \int T_C^{3D}(z)\,dz \int \frac{p(z)^2}{p_s^2}\,dz \quad (1)$$

where T_C^{3D} is the Curie temperature obtained from the conventional p-d Zener model, $p(z)$ the hole density distribution along the z-direction, and p_s the sheet hole density. Although $p(z)$ cannot be measured directly, it is calculated self-consistently. The 1D Poisson equation is numerically solved to determine $p(z)$, considering that the Fermi level of (Ga,Mn)As and the highest occupied molecular orbitals (HOMOs) of the organic molecules align with each other. In the numerical calculation, a certain number of positive interface states residing at molecule/(Ga,Mn)As boundary is also used as an adjustable parameter. Figure 4b shows the calculated $p(z)$ for a 9 nm thick (Ga,Mn)As film with various ΔE, the energy difference between the Fermi level of the (Ga,Mn)As and HOMO of the organic molecules. Here, the acceptor concentration $N_a = 4 \times 10^{19}$ cm^{-3} (similar to the experimental value) and positive interface states $N_i = 1 \times 10^{13}$ cm^{-2} are used. The corresponding log(T_C) versus log(p) curve is shown in Figure 4c, which yields a slope of about 0.11. The simulation results for several film thicknesses plotted in the inset of Figure 4c show a monotonic decrease of γ with the film thickness and good agreement with the experimental values. Furthermore, the resulting calculation of T_C and p show a correlation consistent with our experimental data.

In summary, we have demonstrated a new method for effective tuning of the ferromagnetism in III–V DMS via surface decoration of organic molecules. Both enhancement and suppression of the ferromagnetism are realized by using electron acceptor and donor molecules, respectively. The range of T_C modulation reaches an unprecedented 36 K. Simultaneous magnetic and Hall measurements reveal a close correlation between the surface molecule induced variations of the magnetic properties and the hole density in the (Ga,Mn)As films. The results suggest that the mechanism for the molecular modulation of magnetism is via variation of the hole concentration, which is supported by numeric simulations based on the

modified p-d Zener model. The experiments point to a novel pathway for nanoscale manipulation of ferromagnetism using nanopatterns of organic molecules. Especially, successful DPN of MHA on (Ga,Mn)As offers the possibility of a convenient method of generating arbitrary and reconfigurable magnetic nanostructures, which may find applications in magnetic storage and molecular spintronic devices based on DMSs.

Experimental Section

Film Growth: All the (Ga,Mn)As films used in this study (nominal M_n concentration of 4%, thicknesses = 5–10 nm, and GaAs cap layers = 0–2 nm) were grown by LT-MBE at substrate temperature T_S = 250 °C, on top of a 150 nm GaAs (001) buffer layer. No evidence of precipitation of any secondary phase could be observed during deposition by reflection high-energy electron diffraction (RHEED) or after deposition by X-ray diffraction. The details for reproducible growth of this kind of high-quality films have been reported in refs. [44] and [46].

Molecular Layer Formation: In the standard passivation treatment, the films were soaked in the 1% $(NH_4)_2S_x$ solution[32–34] for 3 min at 40 °C. The films were then rinsed for 2 min under flowing deionized water and blown dry. After the S-passivation, the samples were dipped in the MHA ethanol solution with concentration of 1×10^{-3} M for 15–20 s to deposit MHA on the entire film, or used as the substrate to create nanopatterns of MHA SAM by DPN. F4-TCNQ (Sigma-Aldrich) thin films with 1–3 nm thick were deposited on freshly grown films by thermal evaporation at a high vacuum $\approx 10^{-4}$ Pa.

DPN Patterning: Deposition of MHA on S-passivated films was achieved by dipping the tip into an MHA–ethanol solution for about 15 s and removing excess solvent with nitrogen gas or absorption by a cleanroom paper. In DPN writing, the AFM was operated in a contact mode with a contact force of ≈1 nN and the tip was moved along the substrate to direct the deposition of MHA monolayer onto the desired region. Finally, the patterned surface was imaged and verified by LFM.

Characterization: The chemical composition and bonding chemistry of various GaAs surfaces were characterized by XPS at room temperature. HRTEM was performed to show that the 2–3 nm native oxide layer was successfully removed, which surrounded the GaAs nanowire (see the Supporting Information). The magnetic and transport measurements were, respectively, performed in a SQUID and a PPMS.

Supporting Information

Supporting Information is available from the Wiley Online Library or from the author.

Acknowledgements

The work described here was supported by the National Natural Science Foundation of China (NSFC, Grant Nos. 11228408, 11404323, and 11127406), and by the CAS/SAFEA International Partnership Program for Creative Research Teams. Work at FSU was supported by NSF DMR Grant No. 1308613.

Received: July 22, 2015
Revised: August 21, 2015
Published online: November 5, 2015

[1] T. Jungwirth, J. Sinova, J. Mašek, J. Kučera, A. H. MacDonald, *Rev. Mod. Phys.* **2006**, *78*, 809.
[2] A. H. MacDonald, P. Schiffer, N. Samarth, *Nat. Mater.* **2005**, *4*, 195.
[3] T. Dietl, H. Ohno, F. Matsukura, J. Cibert, D. Ferrand, *Science* **2000**, *287*, 1019.
[4] H. Ohno, D. Chiba, F. Matsukura, T. Omiya, E. Abe, T. Dietl, Y. Ohno, K. Ohtani, *Nature* **2000**, *408*, 944.
[5] S. Koshihara, A. Oiwa, M. Hirasawa, S. Katsumoto, Y. Iye, C. Urano, H. Takagi, H. Munekata, *Phys. Rev. Lett.* **1997**, *78*, 4617.
[6] Y. Nishitani, D. Chiba, M. Endo, M. Sawicki, F. Matsukura, T. Dietl, H. Ohno, *Phys. Rev. B* **2010**, *81*, 045208.
[7] H.-H. Yang, Y.-H. Chu, C.-I. Lu, T. H. Yang, K.-J. Yang, C.-C. Kaun, G. Hoffmann, M.-T. Lin, *ACS Nano* **2013**, *7*, 2814.
[8] E. Delamarche, B. Michel, H. A. Biebuyck, C. Gerber, *Adv. Mater.* **1996**, *8*, 719.
[9] J. C. Love, L. A. Estroff, J. K. Kriebel, R. G. Nuzzo, G. M. Whitesides, *Chem. Rev.* **2005**, *105*, 1103.
[10] S. Sanvito, *Chem. Soc. Rev.* **2011**, *40*, 3336.
[11] X. Zhang, S. A. McGill, P. Xiong, *J. Am. Chem. Soc.* **2007**, *129*, 14470.
[12] Z. H. Xiong, D. Wu, Z. V. Vardeny, J. Shi, *Nature* **2004**, *427*, 821.
[13] T. S. Santos, J. S. Lee, P. Midgal, I. C. Lekshmi, B. Satpati, J. S. Moodera, *Phys. Rev. Lett.* **2007**, *98*, 016601.
[14] C. Barraud, P. Seneor, R. Mattana, S. Fusil, K. Bouzehouane, C. Deranlot, P. Graziosi, L. Hueso, I. Bergenti, V. Dediu, F. Petroff, A. Fert, *Nat. Phys.* **2010**, *6*, 615.
[15] B. Göhler, V. Hamelbeck, T. Z. Markus, M. Kettner, G. F. Hanne, Z. Vager, R. Naaman, H. Zacharias, *Science* **2011**, *331*, 894.
[16] O. B. Dor, S. Yochelis, S. P. Mathew, R. Naaman, Y. Paltiel, *Nat. Commun.* **2013**, *4*, 2256.
[17] K. V. Raman, A. M. Kamerbeek, A. Mukherjee, N. Atodiresei, T. K. Sen, P. Lazić, V. Caciuc, R. Michel, D. Stalke, S. K. Mandal, S. Blügel, M. Münzenberg, J. S. Moodera, *Nature* **2013**, *493*, 509.
[18] S. Steil, N. Großmann, M. Laux, A. Ruffing, D. Steil, M. Wiesenmayer, S. Mathias, O. L. A. Monti, M. Cinchettiand, M. Aeschlimann, *Nat. Phys.* **2013**, *9*, 242.
[19] N. Atodiresei, J. Brede, P. Lazić, V. Caciuc, G. Hoffmann, R. Wiesendanger, S. Blügel, *Phys. Rev. Lett.* **2010**, *105*, 066601.
[20] M. Callsen, V. Caciuc, N. Kiselev, N. Atodiresei, S. Blügel, *Phys. Rev. Lett.* **2013**, *111*, 106805.
[21] C. Herrmann, G. C. Solomon, M. A. Ratner, *J. Am. Chem. Soc.* **2010**, *132*, 3682.
[22] S. G. Ray, S. S. Daube, G. Leitus, Z. Vager, R. Naaman, *Phys. Rev. Lett.* **2006**, *96*, 036101.
[23] X. Zhang, S. A. McGill, P. Xiong, X. L. Wang, J. H. Zhao, *Appl. Phys. Lett.* **2014**, *104*, 152403.
[24] I. Stolichnov, S. W. E. Riester, H. J. Trodah, N. Setter, A. W. Rushforth, K. W. Edmonds, R. P. Campion, C. T. Foxon, B. L. Gallagher, T. Jungwirth, *Nat. Mater.* **2008**, *7*, 464.
[25] H. Boukari, P. Kossacki, M. Bertolini, D. Ferrand, J. Cibert, S. Tatarenko, A. Wasiela, J. A. Gaj, T. Dietl, *Phys. Rev. Lett.* **2002**, *88*, 207204.
[26] T. C. Kreutz, E. G. Gwinn, R. Artzi, R. Naaman, H. Pizem, C. N. Sukenik, *Appl. Phys. Lett.* **2003**, *83*, 4211.
[27] I. Carmeli, A. Lewin, E. Flekser, I. Diamant, Q. Zhang, J. Shen, M. Gozin, S. Richter, Y. Dagan, *Angew. Chem., Int. Ed.* **2012**, *51*, 7162.
[28] D. Y. Petrovykh, M. J. Yang, L. J. Whitman, *Surf. Sci.* **2003**, *523*, 231.
[29] M. J. L. Sourribes, I. Isakov, M. Panfilova, P. A. Warburton, *Nanotechnology* **2013**, 24, 045703.
[30] T. Takenobu, T. Takano, M. Shiraishi, Y. Murakami, M. Ata, H. Kataura, Y. Achiba, Y. Iwasa, *Nat. Mater.* **2003**, *2*, 683.
[31] N. Koch, S. Duhm, J. P. Rabe, A. Vollmer, R. L. Johnson, *Phys. Rev. Lett.* **2005**, *95*, 237601.
[32] D. Kim, S. Cho, N. P. Butch, P. Syers, *Nat. Phys.* **2012**, *8*, 459.
[33] C. Coletti, C. Riedl, D. S. Lee, B. Krauss, L. Patthey, K. von Klitzing, J. H. Smet, U. Starke, *Phys. Rev. B* **2010**, *81*, 235401.

[34] H. A. Budz, M. C. Biesinger, R. R. LaPierre, *J. Vac. Sci. Technol., B* **2009**, *27*, 637.
[35] R. Stine, D. Y. Petrovykh, *J. Electron Spectrosc. Relat. Phenom.* **2009**, *172*, 42.
[36] R. D. Piner, J. Zhu, F. Xu, S. Hong, C. A. Mirkin, *Science* **1999**, *283*, 661.
[37] P. E. Sheehan, L. J. Whitman, *Phys. Rev. Lett.* **2002**, *88*, 156104.
[38] S. H. Hong, J. Zhu, C. A. Mirkin, *Science* **1999**, *286*, 523.
[39] A. Ivanisevic, C. A. Mirkin, *J. Am. Chem. Soc.* **2001**, *123*, 7887.
[40] S. E. Kooi, L. A. Baker, P. E. Sheehan, L. J. Whitman, *Adv. Mater.* **2004**, *16*, 1013.
[41] K. T. Lee, Y. S. Jung, S. M. Oh, *J. Am. Chem. Soc.* **2003**, *125*, 5652.
[42] M. Sawicki, D. Chiba, A. Korbecka, Y. Nishitani, J. A. Majewski, F. Matsukura, T. Dietl, H. Ohno, *Nat. Phys.* **2010**, *6*, 22.
[43] M. A. Mayer, P. R. Stone, N. Miller, H. M. Smith III, O. D. Dubon, E. E. Haller, K. M. Yu, W. Walukiewicz, X. Liu, J. K. Furdyna, *Phys. Rev. B* **2010**, *81*, 045205.
[44] L. Chen, X. Yang, F. H. Yang, J. H. Zhao, J. Misuraca, P. Xiong, S. von Molnár, *Nano Lett.* **2011**, *11*, 2584.
[45] T. Dietl, H. Ohno, F. Matsukura, *Phys. Rev. B* **2001**, *63*, 195205.
[46] S. H. Nie, Y. Y. Chin, W. Q. Liu, J. C. Tung, J. Lu, H. J. Lin, G. Y. Guo, K. K. Meng, L. Chen, L. J. Zhu, D. Pan, C. T. Chen, Y. B. Xu, W. S. Yan, J. H. Zhao, *Phys. Rev. Lett.* **2013**, *111*, 027203.